

Neutron, electron, and x-ray scattering investigation of $\text{Cr}_{1-x}\text{V}_x$ near quantum criticalityD. A. Sokolov,^{1,*} M. C. Aronson,^{1,2} L. Wu,¹ Y. Zhu,^{1,2} C. Nelson,¹ J. F. Mansfield,³ K. Sun,³ R. Erwin,⁴ J. W. Lynn,⁴ M. Lumsden,⁵ and S. E. Nagler⁵¹*Brookhaven National Laboratory, Upton, New York 11973, USA*²*Department of Physics and Astronomy, Stony Brook University, New York 11794, USA*³*Department of Materials Science and Engineering, The University of Michigan, Ann Arbor, Michigan 48090, USA*⁴*NIST Center for Neutron Research, NIST, Gaithersburg, Maryland 20899, USA*⁵*Quantum Condensed Matter Division, Oak Ridge National Laboratory, Oak Ridge, Tennessee 37831, USA*

(Received 21 February 2014; revised manuscript received 8 July 2014; published 29 July 2014)

The weakness of electron-electron correlations in the itinerant antiferromagnet Cr doped with V has long been considered the reason that neither new collective electronic states nor even non-Fermi-liquid behavior are observed when antiferromagnetism in $\text{Cr}_{1-x}\text{V}_x$ is suppressed to zero temperature. We present the results of neutron and electron diffraction measurements of several lightly doped single crystals of $\text{Cr}_{1-x}\text{V}_x$ in which the archetypal spin density wave instability is progressively suppressed as the V content increases, freeing the nesting-prone Fermi surface for a new striped charge instability that occurs at $x_c = 0.037$. This novel nesting driven instability relieves the entropy accumulation associated with the suppression of the spin density wave and avoids the formation of a quantum critical point by stabilizing a new type of charge order at temperatures in excess of 400 K. Restructuring of the Fermi surface near quantum critical points is a feature found in materials as diverse as heavy fermions, high-temperature copper oxide superconductors and now even elemental metals such as Cr.

DOI: [10.1103/PhysRevB.90.035139](https://doi.org/10.1103/PhysRevB.90.035139)

PACS number(s): 74.40.Kb, 71.45.Lr

I. INTRODUCTION

A quantum critical point (QCP) is generated when matter undergoes a continuous transition from one state to another at zero temperature under the action of a nonthermal control parameter Γ_c such as external pressure, magnetic field, or chemical doping. The suppression of electronic order to zero temperature would ultimately lead to an entropy singularity at a QCP [1], but the violation of the third law of thermodynamics can be prevented by the formation of novel collective phases, including unconventional superconductivity in heavy fermion materials such as CeCu_2Si_2 [2], CePd_2Si_2 [3], and UGe_2 [4], and “electron nematicity” in $\text{Sr}_3\text{Ru}_2\text{O}_7$ [5]. There is much interest in identifying new compounds that are naturally near QCPs. Materials of this class are important for their exquisite sensitivity to external fields, and the most extremal response occurs when the ordered state is tuned just to the verge of instability, i.e., at a QCP. A primary obstacle to designing materials based on this functionality is the inherent difficulty in connecting the physics of a parent material with that of the modified quantum critical material where the underlying electronic structure is often vastly different.

There are few systems where a Fermi surface (FS) has been tracked from the ordered state to the QCP, and where the underlying electronic structure is simple enough to unambiguously identify the signatures of quantum criticality. A simple electronic structure, a well established experimental and theoretical understanding of the FS, and the itinerant nature of the d electrons all make Cr an ideal material for studies of quantum criticality. Elemental Cr undergoes a spin density wave (SDW) transition to antiferromagnetic (AF) order at 311 K that is driven by the nesting of large, parallel sections of the FS [6]. High pressures suppress the related charge

density wave (CDW), which disappears continuously at the critical pressure $P_C \sim 10$ GP [7]. Strong charge fluctuations transverse to the wave vector of the modulation were reported to destroy the Bardeen-Cooper-Schrieffer state of the SDW, whereas the FS nesting was even improved under pressure. Chemical doping introduces electrons or holes that can change the FS volume and reduce the SDW nesting [6]. We present here a comprehensive experimental study of $\text{Cr}_{1-x}\text{V}_x$ that uses V doping to tune the SDW to a QCP. Neutron diffraction experiments that probe the static magnetic moment and electron diffraction measurements that probe the charge order connect variations in the order parameter and the wave vector of the coupled SDW/CDW instabilities to the electronic structure both near and far from the QCP.

II. EXPERIMENT

Single crystals of $\text{Cr}_{1-x}\text{V}_x$, $x = 0.0, 0.02, \text{ and } 0.037$, were grown by the arc zone melting method at the Materials Preparation Center at the Ames National Laboratory. Neutron diffraction measurements were carried out on these single crystals of $\text{Cr}_{1-x}\text{V}_x$ using the BT-9 triple-axis spectrometer at the National Institute for Standards and Technology Center for Neutron Research, using a fixed final energy $E_F = 14.7$ meV. The measurements were performed using a 40'-47'-42'-82' configuration. Data were collected near the (1,0,0) and (0,1,0) reciprocal lattice positions in the $(HK0)$ plane. Some of our early results were obtained using the HB3 triple-axis spectrometer at the High Flux Isotope Reactor at Oak Ridge National Laboratory. X-ray diffraction measurements were performed using X-16B instrument at the National Synchrotron Light Source at the Brookhaven National Laboratory. Electron microprobe measurements were made at a 20 kV accelerating voltage on a CAMECA SX100 electron microprobe analyzer using Cr and V x-ray lines calibrated with Cr and V standards. TEM measurements were carried out on single crystals of $\text{Cr}_{1-x}\text{V}_x$, $x = 0, 0.02, \text{ and } 0.37$ using JEOL 2010F and

*Corresponding author: dsokolov@staffmail.ed.ac.uk

JEOL 3000F transmission electron microscopes. A GATAN liquid helium holder was used for low-temperature TEM measurements. $\text{Cr}_{1-x}\text{V}_x$ samples were electropolished for TEM experiments using a methanol:perchloric acid solution (90:10 by volume) at $T = 260$ K.

III. RESULTS AND DISCUSSION

The SDW in pure Cr is stabilised by the Coulomb attraction between holes and electrons, reinforced by the strong nesting of large parallel parts of their respective FSs [6,8], Fig. 1(a). In a neutron diffraction experiment, the appearance of satellites, Fig. 1(b) near the bcc $h + k + l = \text{odd}$ peaks marks SDW onset at the Néel temperature, T_N . Substituting V for Cr shrinks the electron FS relative to the hole FS, making a smaller fraction of the FS nestable [9–11]. The result is a SDW with a smaller moment and lower T_N . As the mismatch between the hole and electron FS becomes larger, the SDW wave vector Q_{SDW} in the doped $\text{Cr}_{1-x}\text{V}_x$ becomes increasingly incommensurate with the lattice.

SDW formation is accompanied by charge modulation, since electron-phonon coupling can drive a lattice distortion

that reduces the energy cost of the purely electronic part of the SDW. This CDW was previously detected in both x-ray and neutron diffraction experiments [7,12–15] on pure Cr as additional superlattice peaks with $Q_{\text{CDW}} = 2Q_{\text{SDW}}$ that appear with the SDW superlattice peaks at T_N . Our x-ray diffraction experiments confirmed CDW in Cr with $Q_{\text{CDW}} = 2\pi/a(2.09, 0, 0)$, Fig. 1(d). We have used transmission electron microscopy (TEM) experiments to study CDW formation in Cr, Fig. 1(c) [16], confirming that $Q_{\text{CDW}} \simeq 2Q_{\text{SDW}}$ [Fig. 1(c)] and that the CDW is present at 300 K but absent at 350 K, as expected given that $T_N = 311$ K in bulk Cr. Taken together, the neutron, x-ray, and TEM experiments confirm that corresponding CDW and SDW modulations are present in pure Cr, arising from the same nesting-driven FS instability.

The aim of the experiments presented here is to determine whether this scenario is still appropriate when the SDW instability is driven to very low temperatures by replacing Cr by nonisoelectronic V in $\text{Cr}_{1-x}\text{V}_x$. High pressures suppress the SDW by increasing the breadth of the nested band [17], while V doping reduces the volume of the Γ -centered electron FS, while increasing the volume of the hole FS that is centered at H, Fig. 1(a). Electrical transport and specific heat measurement [18,19] showed that $T_N \rightarrow 0$ for a critical V doping $x_C \simeq 0.04$. Only recently [17] have neutron diffraction experiments begun to probe the vicinity of the doping-induced QCP, and our measurements show that both the SDW wave vector and ordered moment continue to decrease smoothly with T_N as $x \rightarrow x_C$.

We have performed neutron diffraction measurements on $\text{Cr}_{1-x}\text{V}_x$ with $x = 0, 0.02$, and 0.037 , Fig. 2. The superlattice peak for the sample with $x = 0.037$ occurs with $Q_{\text{SDW}} = 0.922 \pm 0.001$ r.l.u., and is only present below the same $T_N = 19$ K [inset, Fig. 2(a)] found in electrical resistivity measurements [20], while its breadth indicates that SDW order persists over a length scale that exceeds 34 Å. Figure 2(b) shows that the ordered moment decreases and the SDW becomes increasingly incommensurate as V doping drives $T_N \rightarrow 0$, consistent with the shrinking of the Γ electron FS and the H hole FS with doping represented in Fig. 1(a). Powder and single-crystal neutron diffraction and other techniques such as electrical resistivity, thermal expansion, and magnetic susceptibility all agree that T_N vanishes approximately linearly at $x_C = 0.040 \pm 0.001$ [Fig. 2(c)]. The amount of nested FS can be modified by electron (Mn) or hole (V) doping, and our results extend earlier measurements [10,21] into the quantum critical region [Fig. 2(d)], confirming that a QCP occurs when the electron FS in Cr drops below a critical size.

If FS survives once the SDW is destabilized, it is interesting to ask whether it persists well into the paramagnetic phase with $x \geq x_C$ where we have carried out TEM experiments on $\text{Cr}_{1-x}\text{V}_x$ ($x = 0.037$). Since we have no *a priori* reason to expect any sort of charge ordering for $T \gg T_N$, the results are very surprising. New diffraction peaks are found [Fig. 3(a)] at all temperatures from 88 to 400 K, corresponding to a superlattice peak with $Q_{\text{SL}} = 1.661 \pm 0.001$ r.l.u., as well as its second harmonic with $2Q_{\text{SL}}$, indicating that the corresponding charge modulation is not purely sinusoidal, but somewhat flat-topped, Fig. 3(b).

To establish the origin of the missing satellite reflections near $\bar{1}10$, $1\bar{1}0$, and $0\bar{2}0$, in Fig. 3 we have calculated the electron

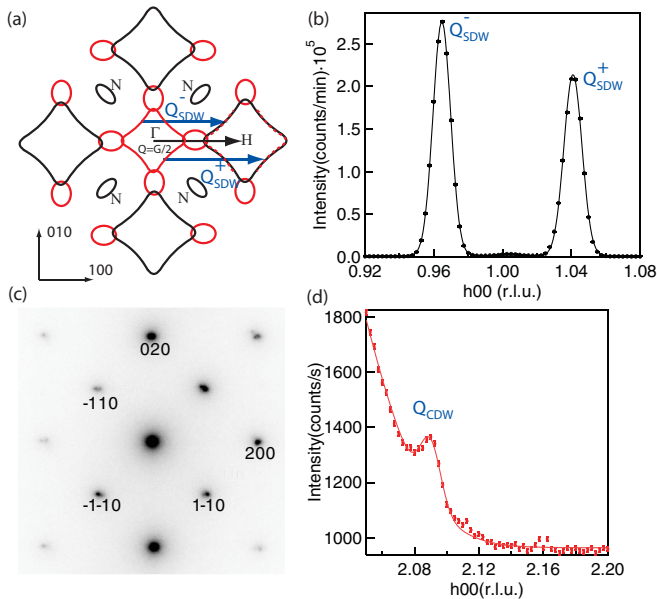


FIG. 1. (Color online) Magnetic and charge modulation in Cr. (a) Nesting of the Γ (electron) and H (hole) FS sheets of Cr by vectors Q_{SDW}^+ and Q_{SDW}^- . Electron lenses located along the vertices of the electron octahedron and hole pockets at N do not contribute to static SDW order. (b) SDW satellites at Q_{SDW}^+ and Q_{SDW}^- in a 300 K neutron diffraction scan in pure Cr along the $[h00]$ direction near the bcc extinct $1,0,0$ Bragg peak. The intensities of the peaks at $Q_{\text{SDW}} = 2\pi/a(1 \pm \delta_{\text{SDW}}, 0, 0)$ obey the magnetic form factor, as expected for the Cr SDW [10]. (c) $(h,k,0)$ plane from the TEM experiment on Cr at 300 K, where the apparent elongation of the $\bar{1}10$ Bragg peak arises from incommensurate CDW satellites that are only present below T_N at $Q_{\text{CDW}} = 2Q_{\text{SDW}}$. (d) CDW satellite at Q_{CDW}^+ in a 300 K x-ray diffraction scan along $[H00]$ near the $2,0,0$ Bragg peak. The incommensurability of CDW $\delta_{\text{CDW}} = 0.090 \pm 0.01$ r.l.u., which is close to $2\delta_{\text{SDW}} = 0.082 \pm 0.024$ taken from the neutron diffraction measurements in (b). Solid lines in (b) and (d) are the best fits to Gaussian line shapes.

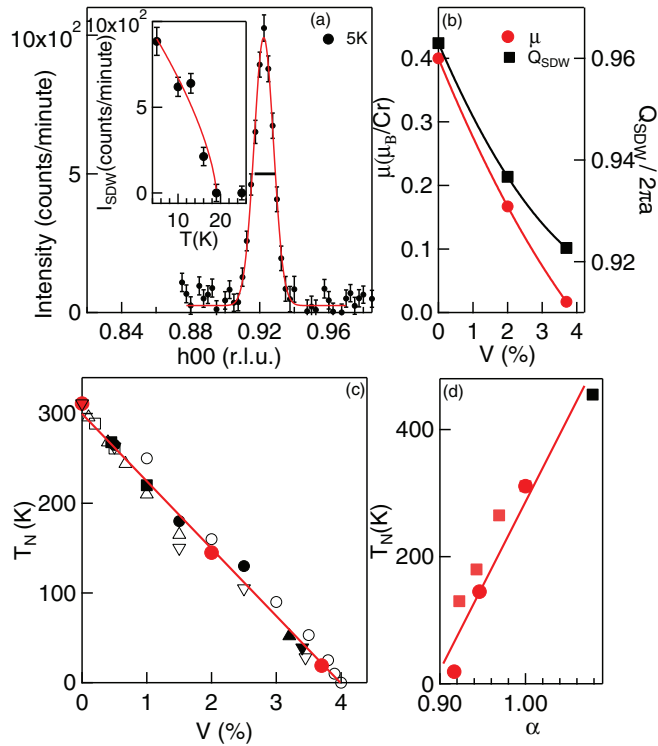


FIG. 2. (Color online) Suppression of the SDW in $\text{Cr}_{1-x}\text{V}_x$. (a) $[h00]$ neutron elastic scan in $\text{Cr}_{0.963}\text{V}_{0.037}$ near the bcc extinct $(1,0,0)$ Bragg peak at 5 K. Solid line is best fit to a Gaussian line shape. Inset shows the temperature dependence of the intensity I_{SDW} of the SDW satellite at $Q = (0.922,0,0)$ r.l.u., which vanishes at $T_N = 19$ K. Solid line is a power law fit. (b) Ordered SDW moments μ and wave vectors Q_{SDW} for $x = 0, 0.02,$ and 0.037 . (c) Neel temperatures T_N for $\text{Cr}_{1-x}\text{V}_x$ determined from our measurements (red filled circles) and from [18] (\circ), [10] (\bullet), [11] (\blacksquare), [22] (\square), [23] (\triangle), [19] (\blacktriangle), [9] (∇), [24] (\blacktriangledown). Linear fit has $T_N \rightarrow 0$ for $x_c = 0.040 \pm 0.001$. (d) Neel temperature as a function of α , the ratio of the total FS area nested in $\text{Cr}_{1-x}\text{V}_x$, and $\text{Cr}_{1-x}\text{Mn}_x$ alloys to the total FS area gapped in pure Cr. Values of T_N taken from neutron diffraction measurements (this work: red filled circles), and from more lightly V-doped samples [10] (red squares) and from a Mn-doped sample [21] (\blacksquare). Line is a guide for the eye. Error bars in (b)–(d) are the size of the symbols.

diffraction patterns for samples with increasing thickness using the dynamical Bloch wave method for a $3 \times 1 \times 1$ superstructure of Cr, Fig. 4. A cosine wave displacement modulation was introduced for superlattice reflections (SLR). The patterns were convoluted with a Lorentzian spread function. At small sample thickness, e.g., in Fig. 4(a), the dynamical coupling among the reflections was weak and the electron diffraction was similar to the x-ray diffraction. The intensities of the superlattice reflections SLR at left (SLR_{200L}) and right (SLR_{200R}) of the 200 reflection were almost the same, though both intensities were very weak. For a thicker sample, e.g., in Fig. 4(b), the dynamical effect multiplying the intensity was stronger than in Fig. 4(a). Some SLRs are enhanced more strongly than the others due to their different excitation errors or deviations from the Ewald’s sphere, resulting in strong asymmetry of the SLRs at the left and right of the main reflections, Fig. 4(d). At large thickness, e.g., in Fig. 4(c), the SLR_{200R} was not observed. We conclude that the

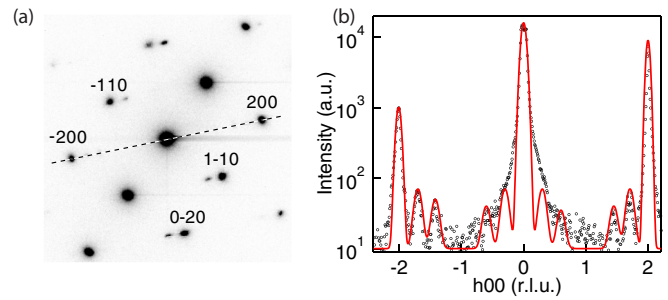


FIG. 3. (Color online) Charge modulation in $\text{Cr}_{0.963}\text{V}_{0.037}$. (a) $(h,k,0)$ reciprocal plane at 300 K, where the characteristic splitting of the bcc Bragg peaks corresponds to a new charge modulation. The dashed line is the direction of the line cut shown in (b). (b) Line cut in the $[h00]$ direction in the reciprocal plane, showing the $(2,0,0)$ and $(\bar{2},0,0)$ r.l.u. bcc Bragg peaks, each with superlattice peaks with $Q_{\text{SL}} = 1.661 \pm 0.001$ r.l.u., and their second harmonics with $2Q_{\text{SL}}$. This solid line is a simulation of the line scan, where the lattice Bragg peaks, as well as the first and second harmonics of the charge modulation, are modeled as Lorentzian-shaped peaks.

relative intensities of the SLRs strongly depend on the sample thickness and differ considerably as the thickness increases as shown in Fig. 4(e).

A real space image of the charge modulation shown in Fig. 3(a) is depicted in Fig. 5(a). The image shows a striplike modulation with a wavelength $\lambda_{\text{SL}} \simeq 3 \pm 0.3a$. The SDW modulation in this $x = 0.037$ sample has

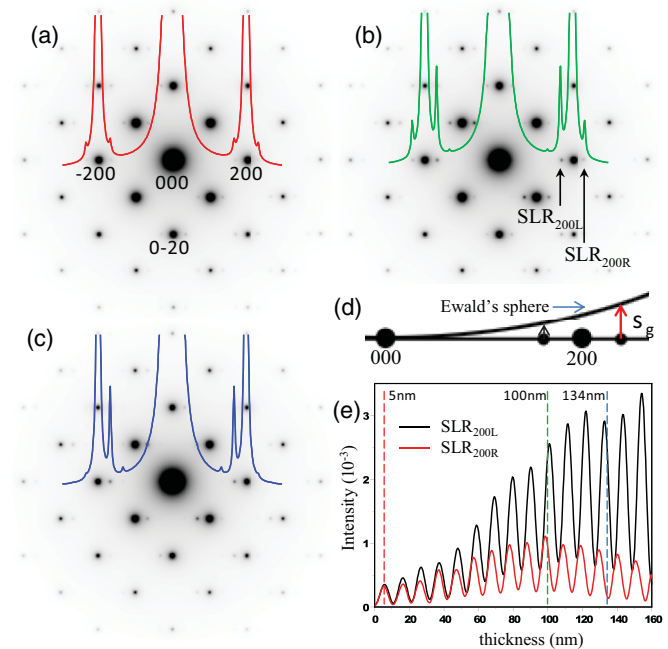


FIG. 4. (Color online) (a)–(c) Calculated $[001]$ electron diffraction patterns with (a) thickness = 5 nm, (b) thickness = 100 nm, and (c) thickness = 134 nm. The embedded lines in (a)–(c) are the intensity line scans from -200 to 200 . (d) Schematics of Ewald’s sphere in the vicinity of 200 reflection, showing that the excitation error, S_g , of SLR_{200L} is smaller than that of SLR_{200R}. (e) Intensities of SLR_{200L} and SLR_{200R} as a function of thickness.

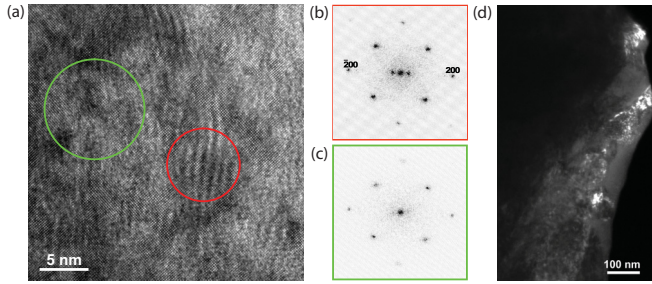


FIG. 5. (Color online) Charge stripes in quantum critical $\text{Cr}_{0.963}\text{V}_{0.037}$. (a) Direct space image with atomic resolution showing long vertical fringes that extend over length scales of ≈ 5 nm. The region inside the red circle has charge stripe modulation; the region inside the green circle represents the unmodulated matrix. (b) The diffraction patterns obtained from the fast Fourier transform (FFT) of the real space image are different for the stripe regions (red circle) and for the matrix in which they are embedded (green circle). The FFT of the striped area encircled in red shows two incommensurate superlattice satellites near $(0,0,0)$. (c) The FFT of the green encircled area shows no satellites, only the bcc Bragg peaks. (d) 300 K dark field image where the bright regions indicate parts of the sample with enhanced intensity at $Q = Q_{SL}$.

$Q_{SDW} = (0.922 \pm 0.001, 0, 0)$ r.l.u., and its corresponding CDW would have $Q_{CDW} = 2Q_{SDW} = (1.844, 0, 0)$ r.l.u., yielding $\lambda_{CDW} \approx 6.4a$, which is about twice the wavelength of the new striped modulation. Both are considerably shorter than the CDW wavelength of $\approx 13a$ found in pure Cr at 300 K. This new striped modulation is unrelated to the SDW/CDW found for $T \leq T_N = 19$ K, or from the Cr inclusions found in this sample. Similarly the absence of a SDW with $Q_{SDW} = 0.5Q_{SL}$ indicates that the striped instability affects only the charge and not the magnetic moment.

Figure 5(a) shows that the striped phase is not spatially homogeneous, but is restricted to regions whose average size is ≈ 5 nm, where Q_{SL} is virtually identical in every region measured. The FFT of the striped regions [Fig. 5(b)] produced clear incommensurate satellites at the same wave vector Q_{SL} in each region tested. No superlattice peaks were observed in the matrix [Fig. 5(c)], which we conclude is simply the paramagnetic metal expected for this composition and temperature. The dark-field image [Fig. 5(d)] shows that about 20–25% of the imaged area is in the striped phase having Q_{SL} parallel to the indicated $[h00]$ direction. Assuming that there is some angular distribution of Q_{SL} that prohibits all striped regions from being imaged simultaneously, the actual volume fraction may be considerably larger.

The general morphology revealed in Fig. 5, where regions with charge order are embedded in a matrix with exemplary crystalline order but no charge superlattice, is reminiscent of the phase separation that accompanies first-order transitions. One source may be the spinodal decomposition of a binary alloy that occurs on cooling from the melt, producing regions that are V deficient and V rich, relative to the average V concentration x_C . In this scenario, the V concentration in the matrix $x_C^- \leq x_C$, and so a SDW would be present for $T \leq T_N = 19$ K. Conversely, the absence of a second SDW in the temperature range $19 \leq T \leq 400$ K implies that the striped

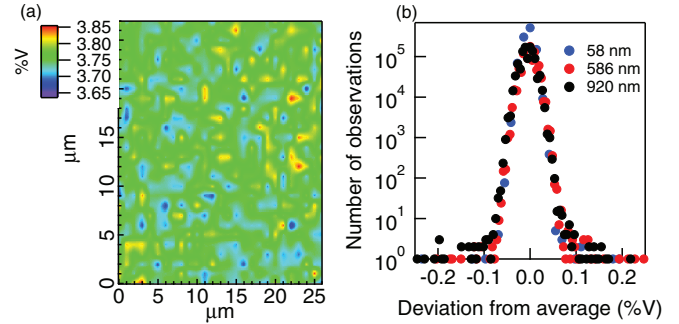


FIG. 6. (Color online) (a) Contour plot of the spatial variation of V concentration obtained from microprobe measurements. The V concentration varies by no more than 4% over the selected area. (b) Histogram of electron energy loss spectroscopy measurements: number of observations for a given V concentration versus deviations from the average V concentration probed on length scales from 58 to 920 nm. The average deviation from the mean V concentration is less than 0.1% for length scales from 58 to 920 nm.

regions would have a V concentration x_C^+ that is larger than x_C . We have used electron microprobe [Fig. 6(a)] and electron energy loss spectroscopy [Fig. 6(b)] to demonstrate that the V concentration varies by no more than 1000 ppm on any length scale larger than ≈ 58 nm, and the lack of variability in λ_{SL} among different striped regions suggests that this is likely also true for length scales that approach the average 5 nm size of the striped regions themselves. Indeed, the binary phase diagram [25] implies continuous solubility of V in Cr, arguing against compositional phase separation. It is more likely [26,27] that the droplets of charge-ordered phase in a uniform SDW matrix represent the coexistence region of a first-order transition that separates the SDW/CDW found for $x \leq x_C$ from an instability that affects only the charge that is found for $x \geq x_C$.

What is the nature of the striped charge modulation that replaces the familiar SDW in Cr for $x \geq x_C$? Initially the FS nesting wave vector in pure Cr connects two different sheets of the FS. The number of nested states decreases with V doping, and eventually is not sufficient to make this SDW/CDW energetically favorable when $x \geq x_C$. The failure of the original SDW/CDW leaves the FS ungapped. The electronic structure calculations for paramagnetic Cr suggest that the FS nesting can occur at multiple vectors either along $[011]$ or $[111]$ [28]. Indeed, the inelastic neutron scattering reported multiple Kohn anomalies in the phonon spectrum of pure Cr, which can soften in doped Cr, stabilizing CDW [29]. More recently, inelastic x-ray scattering experiments with a superior wave vector resolution found softening of phonons in pure chromium that occur far from the established wave vectors of the Fermi surface [30]. The study suggests that the strong electron-phonon coupling alone can drive the phonon softening without invoking Fermi surface nesting. We note, however that q_{SL} is parallel to $[h00]$ in Figs. 3(a) and 5(b), whereas the wave vector of the soft phonon occurs at $q = (0.5, 0.5, 0)$ suggesting either change of the topology of the electron balls and hole lenses or rotation of the electron jack relative to undoped Cr. Whether charge modulation in $\text{Cr}_{0.963}\text{V}_{0.037}$ originates from hidden Fermi surface nesting or is due to soft phonon remains an open question.

Although the binary phase diagram for Cr-V may argue otherwise, it is even possible that the striped regions form in a new binary compound $\text{Cr}_{1000}\text{V}_{38}$, and that this new chemical periodicity is amplified by nesting to result in the formation of the CDW gap, analogous to the FS-driven superstructures seen in other binary compounds such as Cu-Au or Au-Mn, in which a substantial element substitution stabilizes a new charge modulation [31]. Why is this instability, which affects only the charge and not the magnetic moment, absent in pure Cr? It has been suggested [19] that it may exist dynamically, as a pseudogap akin to those discussed in more complex systems such as dichalcogenide [32] and cuprate [33], only becoming a static and incommensurate CDW once the SDW is completely suppressed. The most powerful evidence for the electronic transformation of $\text{Cr}_{1-x}\text{V}_x$ at the QCP comes from Hall effect measurement [19,34], which shows that the number of carriers approximately doubles with the demise of the SDW at x_C , giving a $T \rightarrow 0$ Hall number $R_H^{-1} = 0.35$ electrons/Cr for $x < x_C$ that is in reasonable agreement with the value $R_H^{-1} = 0.54$ electrons/Cr deduced from electronic structure calculation [35], assuming the complete absence of gapping for both Γ and H FSs.

IV. CONCLUSION

Our results underscore the powerful role that nesting plays in the different phases of $\text{Cr}_{1-x}\text{V}_x$, initially driving the SDW/CDW instabilities familiar from pure Cr, but ultimately replacing them at a critical concentration x_C with a new charge instability. While this system shares many of the common

features of correlated electron systems with competing orders, such as FS volume changes and the adoption of novel ordered states near the QCP, the perennial value of Cr as a benchmark system is that a detailed and experimentally verified understanding of the electronic structure is available, and our studies of the magnetic and charge modulation advance this understanding into a new regime.

ACKNOWLEDGMENTS

D.A.S. and M.C.A. would like to thank A. M. Tsvelik, J. Tranquada, T. M. Rice and S. M. Shapiro for useful discussions. Work at BNL was carried out under the auspices of the U.S. Department of Energy, Office of Basic Energy Sciences under Contracts No. DE-AC02-98CH1886 (M.C.A. and D.A.S.) and DE-AC02-98CH10886 (Y.Z. and C.N.). Work at ORNL (M.L. and S.E.N.) was carried out under the auspices of the U.S. Department of Energy, Office of Basic Energy Sciences, Scientific User Facilities Division. The electron microprobe at the University of Michigan used in this study was partially funded by Grant No. EAR-99-11352 from the National Science Foundation. We acknowledge the support of the National Institute of Standards and Technology, U.S. Department of Commerce in providing the neutron research facilities used in this work. Identification of commercial equipment in the text is not intended to imply recommendation or endorsement by the National Institute of Standards and Technology.

-
- [1] A. W. Rost, R. S. Perry, J.-F. Mercure, A. P. Mackenzie, and S. A. Grigera, *Science* **325**, 1360 (2009).
- [2] W. Assmus *et al.*, *Phys. Rev. Lett.* **52**, 469 (1984).
- [3] N. D. Mathur *et al.*, *Nature (London)* **394**, 39 (1998).
- [4] S. S. Saxena *et al.*, *Nature (London)* **406**, 587 (2000).
- [5] R. A. Borzi *et al.*, *Science* **315**, 214 (2007).
- [6] E. Fawcett, *Rev. Mod. Phys.* **60**, 209 (1988).
- [7] R. Jaramillo *et al.*, *Nature (London)* **459**, 405 (2009).
- [8] A. W. Overhauser, *Phys. Rev.* **128**, 1437 (1962).
- [9] E. Fawcett, H. L. Alberts, V. Yu. Galkin, D. R. Noakes, J. V. Yakhmi, *Rev. Mod. Phys.* **66**, 25 (1994).
- [10] W. C. Koehler, R. M. Moon, A. L. Trego, and A. R. Mackintosh, *Phys. Rev.* **151**, 405 (1966).
- [11] S. Komura, Y. Hamaguchi, and M. Kunitomi, *J. Phys. Soc. Jpn.* **23**, 171 (1967).
- [12] Y. Tsunoda, M. Mori, N. Kunitomi, Y. Teraoka, and J. Kanamori, *Solid State Commun.* **14**, 287 (1974).
- [13] Y. Tsunoda, Y. Nakai, and N. Kunitomi, *Solid State Commun.* **16**, 443 (1975).
- [14] R. Pynn, W. Press, and S. M. Shapiro, *Phys. Rev. B* **13**, 295 (1976).
- [15] J. P. Hill, G. Helgesen, and D. Gibbs, *Phys. Rev. B* **51**, 10336 (1995).
- [16] An early TEM report appears in A. F. Prekul and S. V. Sudareva, *Fiz. Met. Metall.* **46**(5), 956 (1978) [*Phys. Met. Metall.* **46**(5), 46 (1979)].
- [17] R. Jaramillo *et al.*, *Phys. Rev. B* **77**, 184418 (2008).
- [18] J. Takeuchi, H. Sasakura, and Y. Masuda, *J. Phys. Soc. Jpn.* **49**, 508 (1980).
- [19] A. Yeh *et al.*, *Nature (London)* **419**, 459 (2002).
- [20] D. A. Sokolov, M. C. Aronson, G. L. Strycker, M. D. Lumsden, S. E. Nagler, and R. Erwin, *Physica B* **403**, 1276 (2008).
- [21] B. J. Sternlieb, E. Lorenzo, G. Shirane, S. A. Werner, and E. Fawcett, *Phys. Rev. B* **50**, 16438 (1994).
- [22] D. R. Noakes, E. Fawcett, and T. M. Holden, *Phys. Rev. B* **55**, 12504 (1997).
- [23] A. J. A. de Oliveira, O. F. de Lima, P. C. de Camargo, W. A. Ortiz, and E. Fawcett, *J. Phys.: Condens. Matter* **8**, L403 (1996).
- [24] R. G. Barnes and T. P. Graham, *J. Appl. Phys.* **36**, 938 (1965).
- [25] T. B. Massalski, H. Okamoto, P. R. Subramanian, and L. Kacprzak, *Binary Alloy Phase Diagrams* (ASM International, Materials Park, OH, 1990), Vols. 1–3.
- [26] J. Burgy, M. Mayr, V. Martin-Mayor, A. Moreo, and E. Dagotto, *Phys. Rev. Lett.* **87**, 277202 (2001).
- [27] Y. J. Uemura *et al.*, *Nat. Phys.* **3**, 29 (2007).
- [28] D. G. Laurent, J. Callaway, J. L. Fry, and N. E. Brener, *Phys. Rev. B* **23**, 4977 (1981).
- [29] W. M. Shaw and L. D. Muhlestein, *Phys. Rev. B* **4**, 969 (1971).
- [30] D. Lamago, M. Hoesch, M. Krisch, R. Heid, K.-P. Bohnen, P. Böni, and D. Reznik, *Phys. Rev. B* **82**, 195121 (2010).

- [31] M. Tachiki and K. Teramoto, *J. Phys. Chem. Solids* **27**, 335 (1966).
- [32] S. V. Borisenko *et al.*, *Phys. Rev. Lett.* **100**, 196402 (2008).
- [33] W. D. Wise *et al.*, *Nat. Phys.* **4**, 696 (2008).
- [34] M. Lee, A. Husmann, T. F. Rosenbaum, and G. Aeppli, *Phys. Rev. Lett.* **92**, 187201 (2004).
- [35] M. R. Norman, Q. Si, Y. B. Bazaliy, and R. Ramazashvili, *Phys. Rev. Lett.* **90**, 116601 (2003).